ACS APPLIED MATERIALS & INTERFACES

Research Article

Cite This: ACS Appl. Mater. Interfaces 2019, 11, 9343−9354

www.acsami.org

Hollow Microspherical and Microtubular [3 + 3] Carbazole-Based Covalent Organic Frameworks and Their Gas and Energy Storage Applications

Ahmed F. M. EL-Mahdy,[†,‡,¶] Christine Young,[§,¶] Jeonghun Kim,[*,∥] Jungmok You,[⊥] Yusuke Yamauchi,[∥,⊥] and Shiao-Wei Kuo[*,†,#]

[†]Department of Materials and Optoelectronic Science, Center of Crystal Research, National Sun Yat-Sen University, Kaohsiung 80424, Taiwan

[‡]Chemistry Department, Faculty of Science, Assiut University, Assiut 71516, Egypt

[§]International Research Center for Materials Nanoarchitechtonics (WPI-MANA) and International Center for Young Scientists (ICYS), National Institute for Materials Science (NIMS), 1-1 Namiki, Tsukuba, Ibaraki 305-0044, Japan

[∥]School of Chemical Engineering & Australian Institute for Bioengineering and Nanotechnology (AIBN), The University of Queensland, Brisbane, Queensland 4072, Australia

[⊥]Department of Plant & Environmental New Resources, Kyung Hee University, 1732 Deogyeong-daero, Giheunggu, Yongin-si, Gyeonggi-do 446-701, South Korea

[#]Department of Medicinal and Applied Chemistry, Kaohsiung Medical University, Kaohsiung 807, Taiwan

Supporting Information

ABSTRACT: Covalent organic frameworks (COFs) are a family of crystalline porous networks having applications in various fields, including gas and energy storage. Despite respectable progress in the synthesis of such crystalline materials, examples of the use of template-free methods to construct COFs having hollow nano- and microstructures are rare. Furthermore, all reported methods for synthesizing these hollow structural COFs have involved [4 + 2] and [3 + 2] condensations. Herein, we report the synthesis of hollow microspherical and microtubular carbazole-based COFs through template-free, one-pot, [3 + 3] condensations of the novel triamine 9-(4-aminophenyl)-carbazole-3,6-diamine (Car-3NH$_2$) and triformyl linkers with various degrees of planarity. Depending upon the monomer's planarity, a unique morphological variety was observed. A time-dependent study revealed that each COF formed through an individual mechanism depended on the degree of planarity of the triformyl linker; it also confirmed that the hollow structures of these COFs formed through inside-out Ostwald ripening. Our COFs exhibited high Brunauer−Emmett−Teller surface areas (up to ca. 1400 m^2 g^{-1}), excellent crystallinity, and high thermal stability. Moreover, the CO_2 uptake capacities of these COFs were excellent: up to 61 and 123 mg g^{-1} at 298 and 273 K, respectively. The high surface areas facilitated greater numbers of strong interactions with CO_2 molecules, leading to high CO_2 uptake capacities. Moreover, the prepared COFs exhibited redox activity because of their redox-active triphenylamine and pyridine groups, which can be utilized in electrochemical energy storages. Accordingly, such hollow COFs having high surface areas appear to be useful materials for industrial and biological applications.

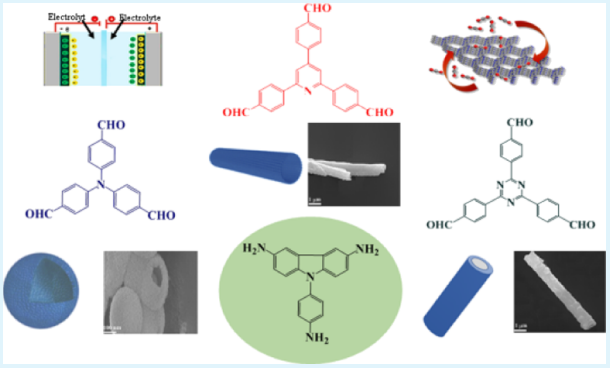

KEYWORDS: *hollow microsphere, hollow microtubule, carbazole, covalent organic framework, CO_2, energy storage*

1. INTRODUCTION

Covalent organic frameworks (COFs) are a new family of crystalline porous organic polymers, possessing lightweight, periodic structures, high surface areas, high thermal stability, and specific pore size distributions.[1−3] COFs can form either two-dimensional (2D) or three-dimensional (3D) structures under dynamic control. For 2D-COFs, the dynamic interplay between covalent bond formation and noncovalent (π-stacking) interactions plays an important role in controlling the crystallinity, structure, and properties of the formed COFs. Relative to amorphous porous polymers, COFs appear to have superior utility in various applications in the fields of optoelectronics,[4] gas storage and separation,[5,6] proton conduction,[7] sensing,[8] catalysis,[9,10] drug delivery,[11] membrane

Received: December 14, 2018
Accepted: February 8, 2019
Published: February 8, 2019

DOI: 10.1021/acsami.8b21867
ACS Appl. Mater. Interfaces 2019, 11, 9343−9354

Scheme 1. Synthesis of Three Car-TPA, Car-TPP, and Car-TPT COFs from Car-3NH$_2$ with Triformyl Linkers Featuring Diverse Planarity

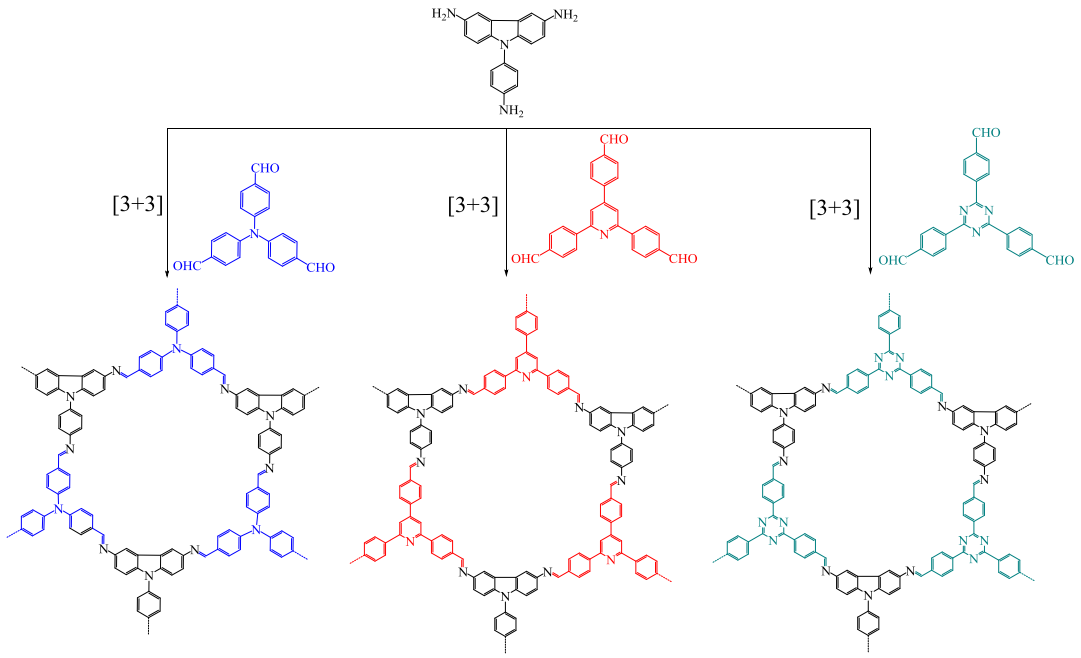

separation,[12] and solar cell.[13] Successful attempts at preparing COFs with good crystallinity have included those using reversible condensation reactions leading to imine,[6,14] hydrazone,[15] triazine,[16] boronate,[17] boroxine,[18] and borosilicate[19] covalent linkages. Although boron-containing COFs have exhibited high degrees of thermal stability, they have not been stable in water or under conditions where they are exposed to moisture.[20,21] In contrast, the imine-, triazole-, and hydrazone-containing COFs have been thermally stable materials that are also highly stable in almost all organic solvents and in water.[15,16,22] The wide availability of organic monomers containing aldehyde (CHO) and amine (NH_2) functional groups, along with the stability of the imine linkage, has led to the construction of many multifunctional imine COFs for a broad range of potential applications. Nevertheless, the discovery of new COFs displaying stability, porosity, and crystallinity remains a challenge.

Carbon dioxide (CO_2) is present in our surrounding atmosphere at a low concentration; the main source of this greenhouse gas is the burning of biomass and fossil fuels.[23,24] The amount of atmospheric CO_2 is increasing daily because of the continuous burning of gas, oil, wood, and coal for energy, and the increasing number of factories to meet human requirements in this industrial age. The detrimental effects of atmospheric CO_2 include increasing sea levels and warming of the global climate; it also has a direct effect on the chemistry and growth of plants. On the other hand, CO_2 has utility as a reaction medium and chemical reagent for the synthesis of many fine chemicals and polymers, including cyclic carbonates,[25] methylacrylic acid, dimethyl ether,[26] and polycarbonates.[27] As a result, the development of new porous materials capable of capturing high amounts of CO_2 with high storage efficiency will have both industrial and academic applications. Recently, COFs have been used as crystalline and porous materials for CO_2 adsorption, displaying high potential for enhanced CO_2 capture capacity.[8,28−30] In particular, Jiang et al. reported that COFs possessing alkyl or carboxylic functional units in their pore walls exhibited massively enhanced CO_2 adsorption capacity as a result of strong interactions with CO_2 molecules.[31,32] Despite many promising advances in the development of COFs, guiding principles for the construction of new COFs targeting excellent CO_2 capture remain elusive.

Much research effort is being devoted to the preparation of COF nanomaterials having specific crystalline shapes and uniform pore size distributions. In most cases, 2D COFs have been synthesized and separated as microcrystalline powders; here, the morphological definition and long-term crystal growth have been restricted because of kinetic trapping and internal disordering of the formed smaller crystallites—the result of the weak π-stacking between COF layers.[33−35] The introduction of stronger π-stacking interactions between COF layers and controlling the rigidity/flexibility of the building monomers will also affect the crystallinity of the resultant COFs.[36−38] COFs have been synthesized in several forms of defined crystallites, including fibers,[39] belts,[4] rectangular prisms,[40] cubes,[19] sheets,[41] platelets,[3] and spheres.[42] Hollow spherical and tubular materials have received much attention for almost a decade because of their potential applications in such fields such as drug delivery,[43,44] catalysis,[45] energy storage, and sensors.[46,47] Hollow spherical and tubular COFs can be constructed using both template-assisted and template-free methods. In the former, an inorganic nanometer-sized metal oxide of a spherical or tubular shape is prepared, used as a template for the growth of a COF on its surface, and then removed.[48,49] In the latter, COFs are self-assembled to form hollow spheres or tubules in the absence of any template; reports on the construction of COFs through this method are exceedingly rare.[10,50,51] Notably, all of the reported template-free methods for the synthesis of hollow spherical and tubular COFs have depended mainly on [3 + 2] and [4 + 2] condensations, respectively. Ding et al. reported the synthesis

DOI: 10.1021/acsami.8b21867
ACS Appl. Mater. Interfaces 2019, 11, 9343−9354

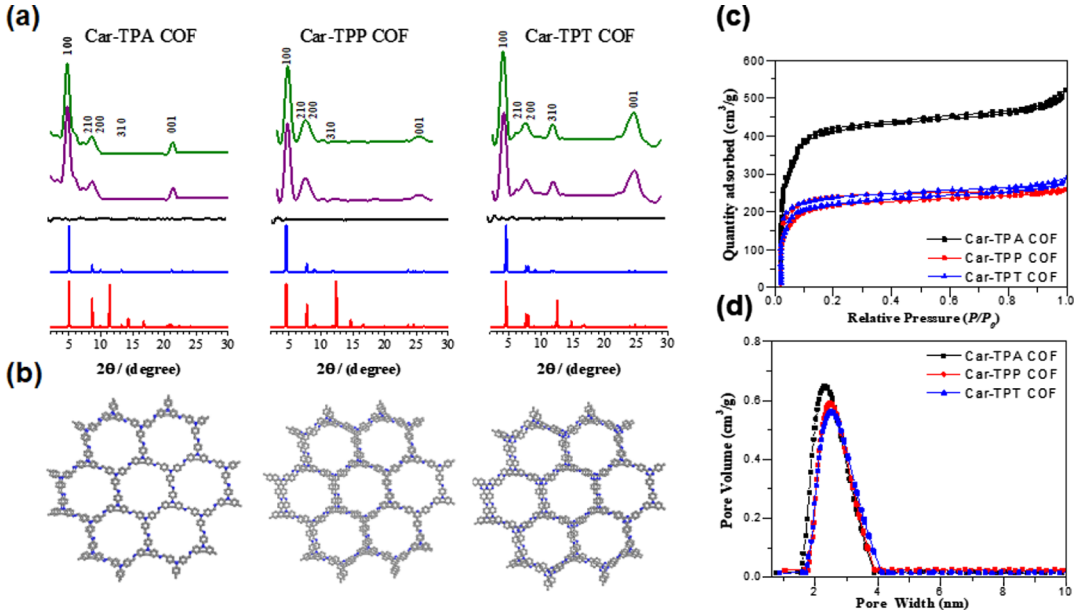

Figure 1. (a) PXRD patterns of Car-TPA, Car-TPP, and Car-TPT COFs: green for the experimentally measured patterns, purple for the simulated patterns that are obtained from the Rietveld refinement, black for the difference between measured and simulated data, and blue and red for the calculated patterns from AA-stacking and AB-stacking, respectively. (b) Space filling model of Car-TPA, Car-TPP, and Car-TPT COFs along the AA-stacking crystalline structures (carbon, gray; nitrogen, blue). (c) Nitrogen adsorption (● filled cycles) and desorption (○ open cycles) isotherms, and (d) pore size distribution profiles of Car-TPA, Car-TPP, and Car-TPT COFs measured at 298 K.

of hollow spherical COF-LZU1, having a Brunauer–Emmett–Teller (BET) surface area of 410 $m^2 g^{-1}$, through the [3 + 2] condensation of 1,3,5-triformylbenzene and 1,4-diaminobenzene.[10] Banerjee et al. reported the synthesis of hollow spherical DhaTab COF, with a BET surface area of 1480 $m^2 g^{-1}$, through [3 + 2] condensation of 1,3,5-tris(4-aminophenyl)benzene and 2,5-dihydroxyterephthal-aldehyde.[50,51] Interestingly, there has been only one reported example of a hollow tubular structure: Beuerle et al. constructed hollow tubular DPP-TAPP COF, having a BET surface area of 139 $m^2 g^{-1}$, through self-assembly and template-free [4 + 2] condensation of 5,10,15,20-tetrakis(4-aminophenyl)porphyrin and diketopyrrolopyrrole.[52]

To the best of our knowledge, the synthesis of hollow spherical and tubular COFs through a template-free, one-pot, [3 + 3] condensation has not been reported previously. Furthermore, the application of hollow spherical and tubular COFs for gas and energy storage has not been examined previously. In this paper, we report the construction of hollow microspherical and microtubular carbazole-based COFs (Car-COFs) having high BET surface areas, up to approximately 1400 $m^2 g^{-1}$, through template-free, one-pot, [3 + 3] condensations (Scheme 1) of a novel 9-(4-aminophenyl)-carbazole-3,6-diamine (Car-$3NH_2$) with triformyl linkers featuring different degrees of planarity, namely tris(4-formylphenyl)amine (TPA-3CHO), 2,4,6-tris(4-formylphenyl)pyridine (TPP-3CHO), and 2,4,6-tris(4-formylphenyl)triazine (TPT-3CHO). Interestingly, the morphology of the Car-COFs depended on the planarity of the triformyl linker. Herein, we describe the mechanisms affecting the morphologies of these structures as well as the suitability of these materials for gas and energy storage.

2. RESULTS AND DISCUSSION

The rigidity and flexibility of the building monomers can play important roles in controlling the crystallinity and shape of the resultant COFs. Thus, in this study we examined the effects of three aromatic triformyl linkers—TPA-3CHO, TPP-3CHO, and TPT-3CHO—displaying different degrees of planarity and flexibility. We applied these aldehydes to the synthesis of Car-TPA COF, Car-TPP COF, and Car-TPT COF through imine formation with the novel triamine Car-$3NH_2$ and investigated the effects of the planarity of the monomers on the morphologies and CO_2 adsorption and energy storage properties of the resulting crystalline COFs. The optimized geometric and energy-minimized structures of these triformyl linkers were obtained through density functional theory (DFT) calculations at the B3LYP/6-311G(d,p) level. TPT-3CHO had the most planar structure, while TPA-3CHO had the least (Table S1).

The new precursor triamine (Car-$3NH_2$) was synthesized through three steps from carbazole, as outlined in Scheme S1. First, carbazole was nitrated with cupric nitrate in a mixture of acetic anhydride and acetic acid at 90 °C to afford a mixture of 1-nitro-, 3,6-dinitro-, and 1,6-dinitro-9*H*-carbazoles, from which the desired 3,6-dinitro-9*H*-carbazole (Car-$2NO_2$) was isolated using column chromatography, eluting with petroleum ether/EtOAc (3:1). 3,6-Dinitro-9-(4-nitrophenyl)-carbazole (Car-$3NO_2$) was then obtained through *N*-arylation of Car-$2NO_2$ with 4-fluoronitrobenzene in dry dimethylsulfoxide (DMSO) in the presence of K_2CO_3 at 140 °C under N_2. Finally, reduction of Car-$3NO_2$ in EtOH, mediated by hydrazine hydrate in the presence of a catalytic amount of 10% Pd/C at 90 °C, afforded Car-$3NH_2$. The chemical structure of Car-$3NH_2$ was confirmed using Fourier transform infrared (FTIR) and ^1H and ^{13}C NMR spectroscopy. The FTIR spectrum of Car-$3NH_2$ featured three sharp signals at 3402, 3337, and 3209 cm^{-1}, representing asymmetric and symmetric NH stretching. The ^1H NMR spectrum of Car-$3NH_2$ (Figure S1) featured two broad signals at 5.25 and 4.66 ppm, attributed to the three NH_2 groups, as well as signals for the aromatic protons in the range from 7.12 to 6.68 ppm. The

DOI: 10.1021/acsami.8b21867
ACS Appl. Mater. Interfaces 2019, 11, 9343–9354

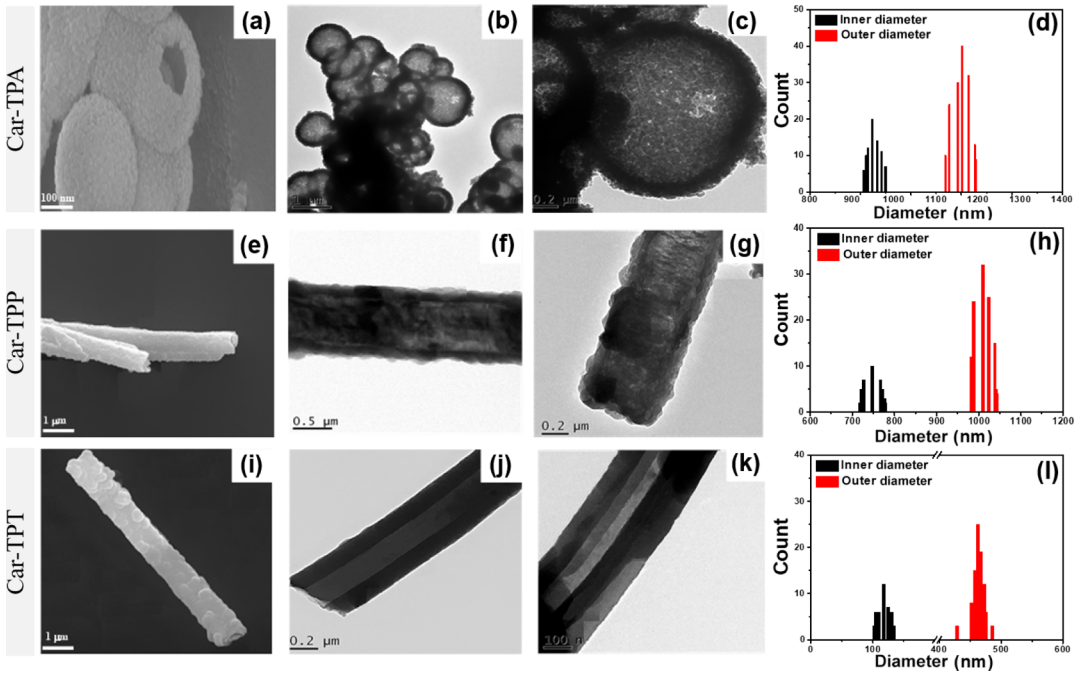

Figure 2. FE-SEM images of (a) hollow spherical Car-TPA, (e) hollow microtubular Car-TPP, and (i) hollow microtubular Car-TPT COFs. TEM images of (b,c) hollow spherical Car-TPA, (f,g) hollow microtubular Car-TPP, and (j,k) hollow microtubular Car-TPT COFs. Statistical distribution data of the inner and outer diameters of (d) Car-TPA, (h) Car-TPP, and (l) Car-TPT COFs.

^{13}C NMR spectrum of Car-3NH$_2$ exhibited two characteristic signals at 147.42 and 141.23 ppm, attributing to the three carbon atoms of the C−NH$_2$ units (Figure S2).

Car-TPA, Car-TPP, and Car-TPT COFs were synthesized under solvothermal conditions through one-pot Schiff-base condensations of Car-3NH$_2$ with TPA-3CHO, TPP-3CHO, and TPT-3CHO (Figures S3−S12), respectively, in dioxane and mesitylene (1:1) in the presence of a catalytic amount of acetic acid (6 M), over 3 days at 120 °C. The resulting Car-COFs were insoluble in common organic solvents, including *N*,*N*-dimethylformamide, acetone, tetrahydrofuran, DMSO, and dioxane. The FTIR spectra of the Car-COFs revealed the complete disappearance of the signals for the amino N−H and aldehydic C═O stretching of the Car-3NH$_2$ and triformyl linkers, while signals appeared for imino C═N stretching at 1621 cm^{-1} (Figures S13−S15), indicating the successful formation of the imine linkages. The compositions of the Car-COFs were confirmed through elemental analysis and solid-state ^{13}C cross-polarization magic angle spinning (CP/MAS) NMR spectroscopy. As listed in Table S2, the found elemental compositions of the three Car-COFs were in agreement with their theoretical values. The ^{13}C NMR spectra of the triformyl linkers (Figures S4, S7, and S12) were characterized by the appearance of a peak at 191.90−191.48 ppm, representing the terminal C═O group; these signals disappeared after condensation with the amine linker to form the three Car-COFs. The ^{13}C NMR spectrum of TPT-3CHO also exhibited a strong peak at 170.47 ppm, representing the triazine unit (Figure S12). The ^{13}C NMR spectra of the three Car-COFs featured characteristic peaks in the range 165.33−161.42 ppm for the resonances of the carbon nuclei of the imino C═N linkages (Figures S16−S19). Notably, the carbon atoms (C−N) bonded directly to the nitrogen atom of the carbazole moiety and the other aromatic carbon atoms were represented by signals in the range from 157.65 to 110.95 ppm. In addition, the ^{13}C NMR spectrum of Car-TPT COF featured a peak at 177.26 ppm, representing the triazine moiety. Thermogravimetric analysis of these Car-COFs revealed that each was thermally stable up to a temperature of 495 °C under a N$_2$ atmosphere (Figure S20, Table S3). Car-TPT COF was the most stable COF, with a value of T_{d10} of 542 °C and a char yield of 55%; for Car-TPA COF and Car-TPP COF, the values of T_{d10} were 495 and 514 °C, respectively, and the char yields were 45 and 58%, respectively. Thus, the presence of the planar triazine moiety appeared to enhance the thermal stability of the resultant COF.

We used powder X-ray diffraction (PXRD), N$_2$ sorption, field-emission scanning electron microscopy (FE-SEM), and transmission electron microscopy (TEM) to gain insight into the crystallinity and morphology of our COFs. The crystallinity of the Car-TPA, Car-TPP, and Car-TPT COFs was confirmed through their PXRD analyses, as displayed in Figures 1a and S21−23. These PXRD patterns indicated the formation of highly crystalline frameworks with hexagonally ordered 2D-honeycomb−type lattices. For Car-TPA COF, an intense diffraction peak appeared at a value of 2θ of 4.9°, corresponding to the 100 reflection, with other minor peaks appearing at 8.6°, 13.1°, and 21.5°, representing the 210, 310, and 001 reflections, respectively. In comparison, Car-TPP COF exhibited a set of PXRD peaks at values of 2θ of 4.3°, 7.3°, 11.4°, and 25.0°, which we assign to the 100, 210, 310, and 001 reflections, respectively. In addition, Car-TPT COF provided a set of PXRD peaks at 2θ values of 4.2°, 7.7°, 12.0°, and 24.9°, which are also assigned to the 100, 210, 310, and 001 reflections, respectively. We used the Bragg equation to calculate the *d*-spacing (d_{100}) between the 100 planes and the π-stacking distance between the 2D stacked sheets. Car-TPA, Car-TPP, and Car-TPT COFs were characterized by d_{100} values of 1.8, 2.0, and 2.1 nm, respectively, and π-stacking distances of 4.1, 3.6, and 3.5 Å, respectively (Table S4). The

DOI: 10.1021/acsami.8b21867
ACS Appl. Mater. Interfaces 2019, 11, 9343−9354

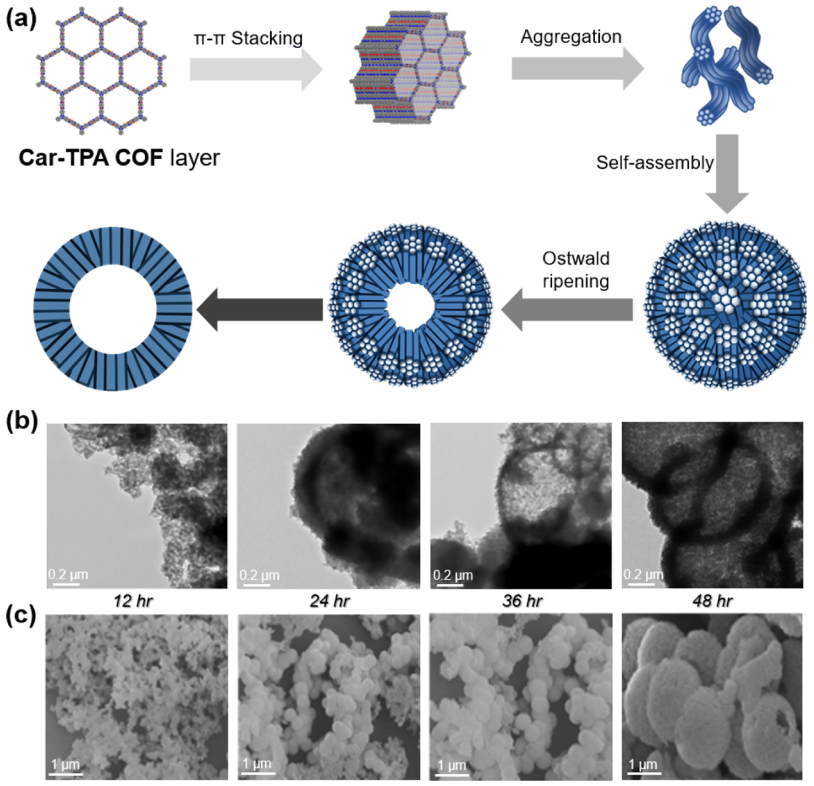

Figure 3. (a) Suggested mechanism of the formation of the hollow spherical Car-TPA COF. (b) TEM and (c) FE-SEM images of the Car-TPA COF measured at different reaction times; 12, 24, 36, and 48 h.

experimentally observed PXRD reflections of the Car-TPA, Car-TPP, and Car-TPT COFs (Figure 1a, green curves) matched well with the theoretical PXRD patterns obtained from the Pawley refinements (Figure 1a, purple curves), as demonstrated by their negligible difference (Figure 1a, black curves). To obtain more information about the conformation of the 2D single layer and the unit cell parameters of the synthesized COFs, we used the program Material studio (v. 6.0) to build AA-eclipsed and AB-staggered stacking models of the Car-TPA, Car-TPP, and Car-TPT COFs. The experimental PXRD patterns of the Car-TPA, Car-TPP, and Car-TPT COFs were in agreement with the simulated PXRD patterns for the AA-eclipsed stacking models but deviated from those of the AB-staggered stacking models. Moreover, the AA-stacking models of the COFs provided the following unit cell parameters: for Car-TPA COF, $a = b = 21.15$ Å, $c = 4.28$ Å, and $\alpha = \beta = 90°$, $\gamma = 120°$; for Car-TPP COF, $a = b = 25.72$ Å, $c = 3.87$ Å, and $\alpha = \beta = 90°$, $\gamma = 120°$; and for Car-TPT COF, $a = b = 27.03$ Å, $c = 4.64$ Å, and $\alpha = \beta = 90°$, $\gamma = 120°$ (Figures S24–S29, Tables S5–S7). Interestingly, the degree of planarity in the triformyl monomer translated well into the crystallinity of the resulting COF; that is, increasing the planarity of the triformyl monomer increased the value of d_{100} and decreased the π-stacking distance between the 2D-stacked sheets.

The N_2 sorption isotherms at 77 K of the activated Car-TPA, Car-TPP, and Car-TPT COFs were recorded to evaluate their permanent porosities. All of the COFs exhibited reversible type I isotherms (Figure 1c)—a characteristic of microporous materials. The surface areas of the Car-TPA, Car-TPP, and Car-TPT COFs, calculated using the BET model, were 1334, 743, and 721 $m^2\ g^{-1}$, respectively, with pore volumes of 0.8, 0.5, and 0.5 $cm^3\ g^{-1}$, respectively. The pore size distributions of the Car-TPA, Car-TPP, and Car-TPT COFs, calculated according to the nonlocal DFT method, revealed that these three COFs were mesoporous materials having pore sizes of 2.3, 2.5, and 2.5 nm, respectively (Figure 1d).

Strikingly, FE-SEM images revealed that the Car-TPA COF assembled into homogenous hollow spheres that were interconnected by means of their mesoporous walls (Figures 2a and S30a–c). A majority of the microspheres were aggregated into a set of bundles; in some cases, however, individual spheres were observed, presumably a result of the sonication applied during the preparation of the sample. On the other hand, the FE-SEM images of the Car-TPP and Car-TPT COFs showed a change in the morphology: to well-defined tubules that also were interconnected by means of their mesoporous walls (Figures 2e,i and S30d–i). Likewise, a majority of the microtubules were aggregated into a set of bundles, but individual microtubules were also present. The morphologies and structures of the Car-TPA, Car-TPP, and Car-TPT COFs were further investigated using TEM. In Figure 2b,c, the TEM images of the Car-TPA COF confirmed the hollow nature and smooth surfaces of the spheres, while the TEM images of the Car-TPP and Car-TPT COFs confirmed their tubular morphologies and the smooth surfaces of their tubules (Figure 2f,g,j,k). Statistical analyses of the TEM images provided mean values for the inner and outer diameters of the spherical structures in the Car-TPA COF of (950 ± 30) nm and (1160 ± 34) nm, respectively (Figure 2d). For the tubular Car-TPP COF, the inner and outer diameters were (750 ± 26) nm and (1008 ± 35) nm (Figure 2h); these values are significantly higher than those of the tubular Car-TPT COF: (117 ± 17) nm and (460 ± 25) nm (Figure 2l). High-resolution TEM images of the three COFs after their liquid exfoliation in butanol revealed the presence of frequent rhomboidal frameworks (Figure S31). Thus, the degree of

DOI: 10.1021/acsami.8b21867
ACS Appl. Mater. Interfaces 2019, 11, 9343–9354

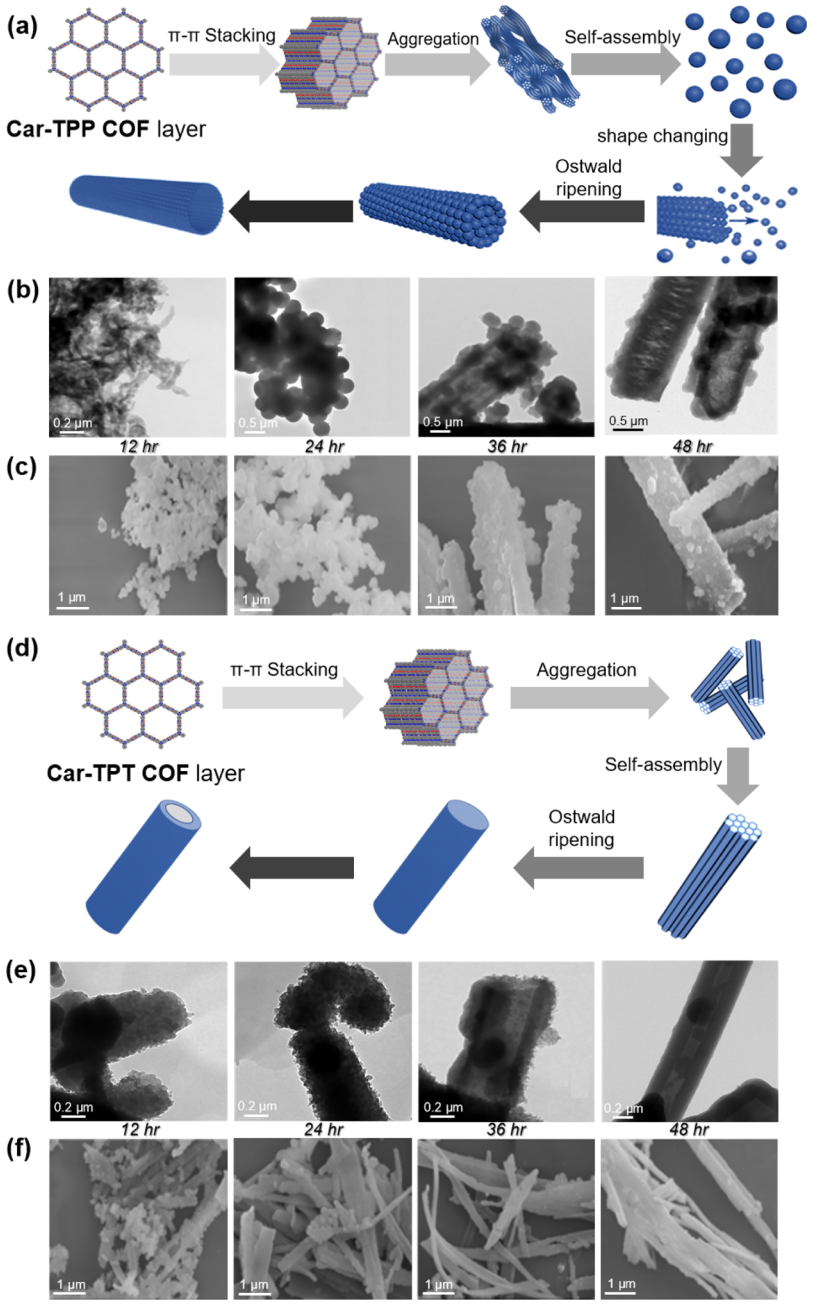

Figure 4. Suggested mechanism of the formation of hollow microtubular (a) Car-TPP COF and (d) Car-TPT COF. TEM images of (b) Car-TPA COF and (e) Car-TPT COF and FE-SEM images of (c) Car-TPP COF and (f) Car-TPT COF measured at different reaction times; 12, 24, 36, and 48 h.

planarity of the three triformyl linkers (TPA-3CHO, TPP-3CHO, and TPT-3CHO) had a strong effect on the crystallite morphology of the resultant COFs; the spherical Car-TPA COF was formed from the least planar TPA-3CHO monomer, while tubular Car-TPP and Car-TPT COFs were produced from the planar TPP-3CHO and TPT-3CHO monomers, respectively. Moreover, increasing the planarity of the monomer decreased the inner and outer diameters of the corresponded COF.

To examine the mechanisms behind the formation of the hollow spheres and tubules, we studied the morphological changes of the three COFs at different times during their formation. The syntheses of Car-TPA, Car-TPP, and Car-TPT COFs were performed under the same solvothermal conditions as before but quenched at 12, 24, 36, and 48 h by cooling to room temperature and isolating the resultant COFs. The morphologies of structures formed at these specific times were analyzed using FE-SEM and TEM imaging (Figures 3 and 4). For the Car-TPA COF, which formed from the least planar TPA-3CHO, the TEM images of the isolated sample at 12 h revealed the formation of small nonspherical and bent fibers having lengths of approximately 150−200 nm and widths of approximately 40−50 nm (Figure 3b). These crystallites presumably formed from π-stacking of the Car-TPA COF layers along the *c*-direction (Figure 3a). After a reaction time of 24 h, these bent crystallites had self-assembled to produce dense and dark spherical structures. The individual bent crystallites, which were used as building units during the

DOI: 10.1021/acsami.8b21867
ACS Appl. Mater. Interfaces 2019, 11, 9343−9354

formation of these dense spheres, were also evident at the outer walls of spheres (Figure 3b). As the reaction time progressed to 36 h, the building crystallites gradually migrated from the center of the sphere to its outer wall, forming a hollow pore inside the dense spheres. Nevertheless, the outer walls of these hollow spheres were not smooth, and the building crystallites remained on the outer walls of the spheres (Figure 3b). Interestingly, the TEM images of the sample isolated after 48 h exhibited completely hollow spheres with smooth outer walls (Figure 3b). We attribute the formation of the smooth outer walls to the Schiff base reactions between the terminal functional groups (aldehydes and amines) on the bent crystallite surface. These TEM images suggested that the main reason for the formation of the hollow spheres was the migration of the crystallites from the sphere centers to the outer wall—the result of inside-out Ostwald ripening.[10,52,53] The formation of hollow spheres through inside-out Ostwald ripening is usually observed for polymer-based spheres[53] and inorganic metal oxides;[54] this process is rarely reported for covalent organic materials. Notably, minimizing the surface energy of the spherical system is the main effect of inside-out Ostwald ripening; crystallites arranged in the inner center, with surface energy higher than that in the outer wall, migrate in the sphere from the center to the outer wall.[55,56]

For the Car-TPP COF, which formed from the planar TPP-3CHO, the sample isolated after a reaction time of 12 h revealed the formation of small stripelike crystallites having lengths of approximately 200−250 nm and widths of approximately 50−55 nm (Figure 4b). As mentioned earlier, the π-stacking distance of Car-TPP COF (3.6 Å) was shorter than that of Car-TPA COF (4.1 Å), indicating that the π-stacking of the Car-TPP COF layers was stronger than that of the Car-TPA COF layers and, thus, induced the formation of more planar stripelike crystallites (Figure 4a). After a reaction time of 24 h, these stripelike crystallites self-assembled into dark and smooth outer spheres. In contrast to the Car-TPA COF, no building stripelike crystallites were evident at the outer walls of these spheres. Interestingly, the dark spheres further self-assembled, after a reaction time of 36 h, into dark microtubules having widths of approximately 970−1040 nm (Figure 4b). This self-assembly into tubules presumably arose from the coalescence of spheres upon Schiff base reactions between the aldehydic and amino groups on the outer surface of each sphere. This mechanism was supported by the observation of dark spheres at the openings of the microtubules (Figure 4b). After 48 h, microtubules with entirely smooth and dark outer walls, and bright contrast within the tubules, had formed, reflecting the formation of hollow tubular structures (Figure 4b). The formation of these hollow tubules was influenced by the migration of spheres from the inner center (where the spheres had higher surface energy) to the outer wall, thereby minimizing the surface energy of whole tubules. Once again, the hollow microtubular morphology of the Car-TPP COF was governed by inside-out Ostwald ripening.

For the Car-TPT COF, which was formed from the most planar TPT-3CHO, TEM images of the sample isolated after a reaction time of 12 h revealed the formation of small stripelike crystallites, having widths of approximately 40−50 nm (Figure 4e). The π-stacking distance of the Car-TPT COF (3.5 Å) was the shortest, compared with the other two, suggesting that its layers possessed the strongest π-stacking and, thus, induced the formation of the most planar stripelike crystallites (Figure 4d). After 24 h, these planar crystallites served as building units that self-assembled to give dense and dark tubular structures. Individual planar crystallites were observed at the outer walls of tubules (Figure 4e). After a reaction time of 36 h, the hollow tubular structures of the isolated sample were formed under the influence of inside-out Ostwald ripening (Figure 4e). Thus, the planar crystallites progressively migrated from the inner center of the tubule to its outer wall, forming tubules with dark outer walls and bright contrast within the tubules (hollow tubular structure). Nevertheless, the outer walls of these hollow tubules were not smooth, and the planar crystallites again were evident on the outer walls of the tubules. After a reaction time of 48 h, the TEM images of the isolated sample revealed completely hollow tubules with smooth outer walls (Figure 4e). Similar to the other cases, we attribute the formation of this smooth outer wall to the Schiff base reactions between the aldehydic and amino units on the planar crystallite surface. The three systems described above confirmed that the morphology of each COF was formed through a different mechanism, which depended on the degree of planarity of the triformyl linker. Such diversity in the COF morphologies and such variations in the mechanisms of formation have not been reported previously.

The synthesis of hollow sphere and hollow tubular COFs occurs infrequently, and is rarely reported; consequently, their applications in various fields are also rarely documented. To the best of our knowledge, the CO_2 adsorption and energy storage of hollow sphere and hollow tubular COFs have never been reported previously. Accordingly, we applied our Car-TPA, Car-TPP, and Car-TPT COFs to studies of their CO_2 adsorption and use in supercapacitors. First, we tested the CO_2 uptake efficiencies of these three COFs at 298 K (Figure 5a)

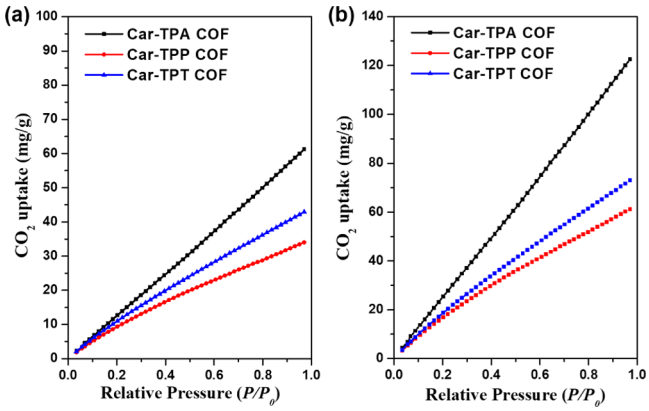

Figure 5. CO_2 uptake profiles of hollow spherical Car-TPA (black), hollow microtubular Car-TPP (red), and hollow microtubular Car-TPT COFs (blue) at (a) 298 and (b) 273 K.

and 273 K (Figure 5b) and up to 1 bar. Among them, the hollow spherical Car-TPA COF displayed the highest CO_2 uptake capacities: 61 and 123 mg g^{-1} at 298 and 273 K, respectively. These capacities were approximately 2- and 1.5-fold higher than those of the Car-TPP and Car-TPT COFs, respectively. The hollow tubular Car-TPT COF provided CO_2 uptake capacities of 42 and 73 mg g^{-1} at 298 and 273 K, respectively; the hollow microtubular Car-TPP COF displayed the lowest CO_2 uptake capacities (34 and 62 mg g^{-1} at 298 and 273 K, respectively). These data suggest that two main factors affected the CO_2 uptakes of our COFs: the surface area

DOI: 10.1021/acsami.8b21867
ACS Appl. Mater. Interfaces 2019, 11, 9343−9354

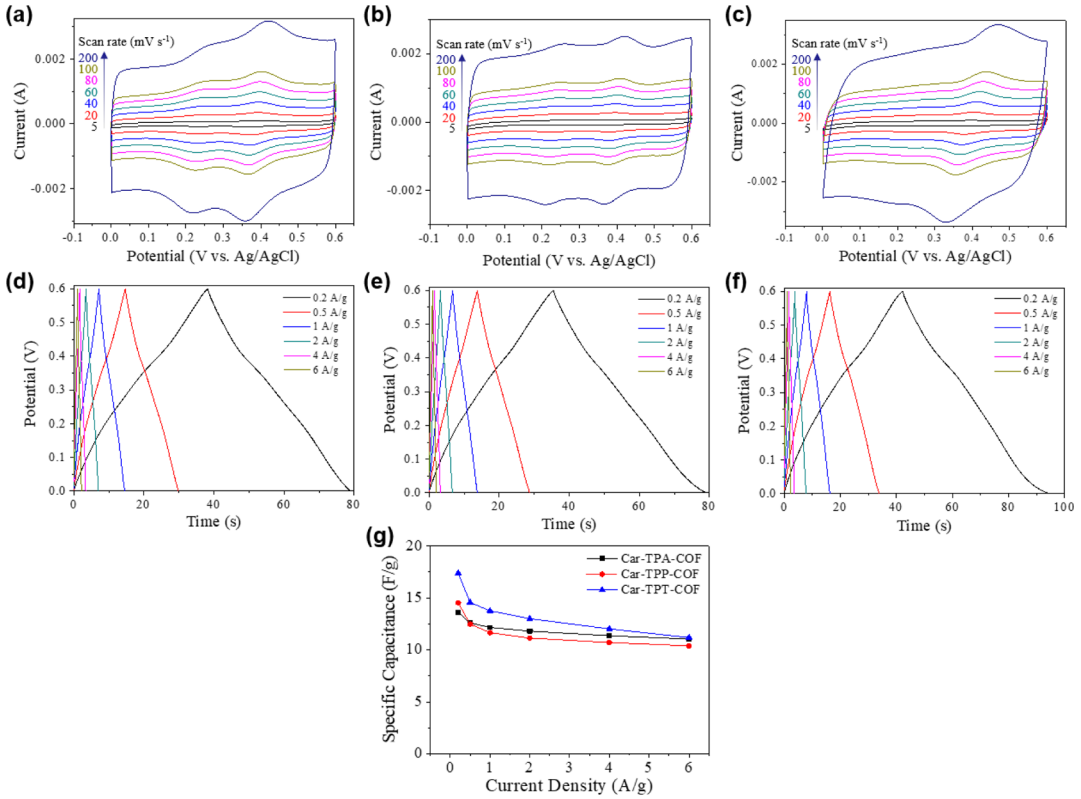

Figure 6. Cyclic voltammograms of (a) Car-TPA, (b) Car-TPP, and (c) Car-TPT COFs at different scan rates in 0.5 M H_2SO_4. GCD curves of (d) Car-TPA, (e) Car-TPP, and (f) Car-TPT COFs at different current densities in 0.5 M H_2SO_4 and (g) specific capacitances of COFs from GCD data at different current densities.

and the nitrogen atom content. The highest surface area Car-TPA COF exhibited the highest CO_2 uptake capacity; in the cases of the Car-TPP and Car-TPT COFs, which had approximately the same surface areas, the atom nitrogen content was the main factor. The Car-TPT COF, having three triazine moieties in its hexagonal pore, had a CO_2 uptake capacity higher than that of the Car-TPP COF, having three pyridine moieties in its hexagonal pore. Interestingly, the CO_2 uptakes of our COFs, especially Car-TPA COF, are among the highest reported COF materials, as shown in Table S8. Boroxine/boronate-based 2D (COF-1, COF-5, COF-6, COF-8, and COF10) and 3D (COF-102, and COF-103) COFs have CO_2 uptakes between 53 and 100 mg g^{-1} at 273 K.[20] In addition, imine-based COFs exhibited CO_2 uptakes between 12 and 63 mg g^{-1} at 298 K and 20 and 118 mg g^{-1} at 273 K.[57−59] Jiang et al. reported the modification of pore walls of COFs with the functionalized group which can enhance the CO_2 uptakes. The hydroxyl- and carboxyl-modified COFs ($[HO]_x$%-H_2P-COFs and $[CO_2H]_x$%-H_2P-COFs) showed CO_2 uptakes between 31 and 76 and 54 and 174 mg g^{-1} at 298 and 273 K, respectively.[60] Further, Jiang et al. reported that ethynyl-, ethyl-, acetate-, acetic-, ethanol-, and amine-modified COFs exhibited CO_2 uptakes between 20−61 and 29−123 mg g^{-1} at 298 and 273 K, respectively.[32] This reported studies indicated that our synthesized COFs have CO_2 uptakes almost similar to the functionalized COFs. Furthermore, we estimated the isosteric heats of adsorption (Q_{st}) of the Car-TPA, Car-TPP, and Car-TPT COFs from their CO_2 adsorption data collected according to the Clausius−Clapeyron equation, at 298 and 273 K. At a low adsorption of CO_2 (ca. 0.1 mmol g^{-1}), the values of Q_{st} of the Car-TPA, Car-TPP, and Car-TPT COFs were 28.4, 20.5, and 21.5 kJ mol^{-1}, respectively. These observed values of Q_{st} confirmed that a higher surface area induced more strong interactions with CO_2 molecules. Considering their almost identical surface areas, the higher value of Q_{st} for the Car-TPT COF, relative to that of the Car-TPP COF, was consistent with the greater nitrogen content (triazine units) in the hexagonal pores of the former COF, enhancing its interactions with the CO_2 molecules.

Our three COFs had redox-active groups—carbazole,[61] pyridine,[62] and triphenylamine[63,64]—on their backbones, making them potentially capable of storing electrochemical energy (Scheme 1). In particular, all of these COFs possessed carbazole groups, while the Car-TPA and Car-TPP COFs additionally featured redox-active triphenylamine and pyridine groups, respectively. We used a three-electrode system to test the redox activities of these COFs through electrochemical measurements in aqueous 0.5 M H_2SO_4. As displayed in Figure 6, cyclic voltammetry (CV) revealed the redox behavior of the COFs, with reversible redox processes occurring in a potential window of 0.0−0.6 V. Only the Car-TPT COF provided a single redox peak because of its carbazole groups. All of the COFs provided CV traces having the shape expected for both electric double-layer capacitance (EDLC) and pseudocapacitance from a high surface area and redox reaction, respectively. We obtained the specific capacitances of three carbazole-based COFs from their galvanostatic charge/discharge (GCD) behavior measured at various current densities (Figure 6). At a current density of 0.2 A g^{-1}, the specific capacitances of the Car-TPA, Car-TPP, and Car-TPT COFs were 13.6, 14.5, and 17.4 F g^{-1}, respectively (Figure 6g). Although the Car-TPA

DOI: 10.1021/acsami.8b21867
ACS Appl. Mater. Interfaces 2019, 11, 9343−9354

COF had the highest surface area (1334 m^2 g^{-1}) and two redox-active groups (carbazole, triphenylamine), it displayed the lowest specific capacitance. Interestingly, the Car-TPT COF, having a surface area of 721 m^2 g^{-1} and only a single redox-active group, displayed the highest capacitance at each current density. This behavior can be explained by considering that the morphological and chemical structural properties of the Car-TPT COF enhanced its specific capacitance. The Car-TPT COF featured an opened microtubular structure (Figure 4), which presumably improved the capacitance and retention during fast charging/discharging because of the efficient accessibility of the electrolyte.[65−67] In addition, the longer units of conjugated bonding induced by the presence of the triazine units on the backbone presumably enhanced the electrical properties—an important factor in the fabrication of electrodes.[68] DeBlase et al.[69,70] reported capacitances of 28 F g^{-1} at 0.2 A g^{-1} and 3.0 mF cm^{-2} at 150 μA cm^{-2} from DAAQ-TFP COFs and Halder et al.[71] reported TpOMe-DAQ exhibiting a capacitance of 135 F g^{-1} at 3.3 mA cm^{-2}. In addition, the TpPa-$(OH)_2$ COF showed a capacitance of 416 F g^{-1} at 0.5 A g^{-1},[72] and TAT-CMP-1 and TAT-CMP-2 revealed 141 and 183 F g^{-1} at 1 A g^{-1}.[68] Most recently, Khayum M et al. reported COF thin sheets for flexible supercapacitors having capacitances of 8.5 mF cm^{-2} (CT−Dq_1Da_1Tp) and 12 mF cm^{-2} (CT−DqTp COF) at 0.39 mA cm^{-2}.[73] The reported capacitance values are summarized in Table S9. Although the capacitances of carbazole-based COFs are lower than those of some other reported COFs, it is noteworthy that new carbazole-based COFs exhibited specific capacitances higher than those of previously reported COFs having same unit, except for that of a COF featuring six triphenyl amine linkages.[57] We conclude that the morphology of a COF material is also an important factor to consider when attempting to improve the specific capacitance. These studies indicate that the molecular design of COFs (i.e. porosity, redox groups, conjugated structure, morphology, etc.) is important for supercapacitor application in terms of redox reaction, surface area, and efficient diffusion.

The chemical stability, porosity, crystallinity, and hollow nature of our synthesized COFs in the aqueous electrolyte (0.5 M H_2SO_4) were investigated by immersing 40 mg of COF material into 10 mL of 0.5 M H_2SO_4 for 3 days. Retention of solid-state ^{13}C CP/MAS NMR peaks (Figure S32) and nonalteration of peaks in the PXRD patterns (Figure S33) after H_2SO_4 treatment indicated the excellent chemical stability and crystallinity of Car-TPA, Car-TPP, and Car-TPT COFs in this aqueous electrolyte. In addition, N_2 adsorption isotherms at 77 K (Figure S34) exhibited that these COFs remained porous after H_2SO_4 treatment with a slight decrease in their BET surface areas; 1334 versus 1250, 743 versus 420, and 721 versus 690 m^2 g^{-1} for Car-TPA, Car-TPP, and Car-TPT COFs, respectively. The FE-SEM images of our COFs showed that the morphology and hollow nature of COFs were also retained after H_2SO_4 treatment (Figure S35). These data confirmed the high stability of synthesized COFs during the electrochemical measurements and applications.

3. CONCLUSIONS

We have synthesized a novel triamine linker (Car-$3NH_2$) and then applied it in the syntheses of three hollow microspherical and microtubular carbazole-based COFs—the Car-TPA, Car-TPP, and Car-TPT COFs—through a one-pot [3 + 3] condensation between Car-$3NH_2$ and triformyl linkers, featuring various degrees of planarity. The resultant Car-COFs exhibited excellent crystallinity, high thermal stability (up to ca. 550 °C), and high BET surface areas (up to ca. 1400 m^2 g^{-1}). According to FE-SEM and TEM imaging, the Car-COFs had morphologies (hollow spheres and hollow tubules) that differed depending upon the degree of planarity of their triformyl linkers. We investigated the mechanisms of formation of these hollow Car-COFs by studying the morphological changes in three COFs at different times during their preparation. Each Car-COF experienced a different mechanism of formation; in addition, the hollow nature of the Car-COFs resulted from inside-out Ostwald ripening. We tested our new Car-COFs for applications related to gas and energy storage. In the case of gas adsorption, these three Car-COFs exhibited excellent CO_2 uptake capacities: up to 61 and 123 mg g^{-1} at 298 and 273 K, respectively. The surface areas and nitrogen atom contents of the linkers played important roles impacting the CO_2 uptake capacity. In the electrochemical measurements, all of the Car-COFs provided CV curves in the shape of both EDLC and pseudocapacitance, confirming the high surface areas and strong redox reactions of the COFs. Interestingly, the triazine-containing Car-TPT COF having an opened microtubular structure displayed the highest specific capacitance (17.4 F g^{-1}) at a current density of 0.2 A g^{-1}. Most importantly, these three new carbazole-containing COFs having hollow morphologies displayed improved specific capacitances relative to those of other reported triphenylamine- and triazine-containing COFs. We hope that such diversity in COF morphologies, and the ease of synthesis of the microtubular COFs, will encourage others to apply these materials in various domains.

■ ASSOCIATED CONTENT

Supporting Information

The Supporting Information is available free of charge on the ACS Publications website at DOI: 10.1021/acsami.8b21867.

Materials, full synthetic procedures, full characterization, 1H-NMR spectrum, ^{13}C-NMR spectrum, FT-IR spectra, ^{13}C cross-polarization magic angle spinning solid-state NMR, Solid-state ^{13}C CP MAS NMR spectra, PXRD pattern, 3D-views, FE-SEM images, TEM images, TGA analyses, solid-state ^{13}C CP MAS NMR spectra, and nitrogen adsorption (● filled cycles) and desorption (○ open cycles) isotherms; DFT geometry optimization of monomers using the B3LYP/6-311G(d,p) method, fractional atomic coordinates, elemental analysis results, $T_d5\%$, $T_d10\%$, and char yield of COFs, and comparison of Car-TPA, Car-TPP, and Car-TPT COFs with other COFs; and additional data (PDF)

■ AUTHOR INFORMATION

Corresponding Authors

*E-mail: jeonghun.kim@uq.edu.au (J.K.).
*E-mail: kuosw@faculty.nsysu.edu.tw (S.-W.K.).

ORCID

Jeonghun Kim: 0000-0001-6325-0507
Jungmok You: 0000-0002-9583-2242
Yusuke Yamauchi: 0000-0001-7854-927X
Shiao-Wei Kuo: 0000-0002-4306-7171

DOI: 10.1021/acsami.8b21867
ACS Appl. Mater. Interfaces 2019, 11, 9343−9354

Author Contributions

[¶]A.F.M.E.-M. and C.Y. contributed equally.

Notes

The authors declare no competing financial interest.

■ ACKNOWLEDGMENTS

This study was supported financially by the Ministry of Science and Technology, Taiwan, under contracts MOST 106-2221-E-110-067-MY3, 105-2221-E-110-092-MY3, and 108-2218-E-110-013-MY3. This work was also performed in part at the Queensland node of the Australian National Fabrication Facility, a company established under the National Collaborative Research Infrastructure Strategy to provide nano and microfabrication facilities for Australia's researchers.

■ REFERENCES

(1) Cote, A. P.; Benin, A. I.; Ockwig, N. W.; O'Keeffe, M.; Matzger, A. J.; Yaghi, O. M. Porous, Crystalline, Covalent Organic Frameworks. *Science* **2005**, *310*, 1166−1170.

(2) Colson, J. W.; Dichtel, W. R. Rationally Synthesized Two-Dimensional Polymers. *Nat. Chem.* **2013**, *5*, 453−465.

(3) El-Kaderi, H. M.; Hunt, J. R.; Mendoza-Cortes, J. L.; Cote, A. P.; Taylor, R. E.; O'Keeffe, M.; Yaghi, O. M. Designed Synthesis of 3D Covalent Organic Frameworks. *Science* **2007**, *316*, 268−272.

(4) Wan, S.; Guo, J.; Kim, J.; Ihee, H.; Jiang, D. A Belt-Shaped, Blue Luminescent, and Semiconducting Covalent Organic Framework. *Angew. Chem., Int. Ed.* **2008**, *47*, 8826−8830.

(5) Du, Y.; Calabro, D.; Wooler, B.; Kortunov, P.; Li, Q.; Cundy, S.; Mao, K. One Step Facile Synthesis of Amine-Functionalized COF-1 with Enhanced Hydrostability. *Chem. Mater.* **2015**, *27*, 1445−1447.

(6) Kandambeth, S.; Mallick, A.; Lukose, B.; Mane, M. V.; Heine, T.; Banerjee, R. Construction of Crystalline 2D Covalent Organic Frameworks with Remarkable Chemical (Acid/Base) Stability via a Combined Reversible and Irreversible Route. *J. Am. Chem. Soc.* **2012**, *134*, 19524−19527.

(7) Xu, H.; Tao, S.; Jiang, D. Proton Conduction in Crystalline And Porous Covalent Organic Frameworks. *Nat. Mater.* **2016**, *15*, 722−726.

(8) Dalapati, S.; Jin, S.; Gao, J.; Xu, Y.; Nagai, A.; Jiang, D. An Azine-Linked Covalent Organic Framework. *J. Am. Chem. Soc.* **2013**, *135*, 17310−17313.

(9) Pachfule, P.; Kandambeth, S.; Díaz Díaz, D.; Banerjee, R. Highly Stable Covalent Organic Framework-Au Nanoparticles Hybrids for Enhanced Activity for Nitrophenol Reduction. *Chem. Commun.* **2014**, *50*, 3169−3172.

(10) Ding, S.-Y.; Gao, J.; Wang, Q.; Zhang, Y.; Song, W.-G.; Su, C.-Y.; Wang, W. Construction of Covalent Organic Framework for Catalysis: Pd/COF-LZU1 in Suzuki-Miyaura Coupling Reaction. *J. Am. Chem. Soc.* **2011**, *133*, 19816−19822.

(11) Fang, Q.; Wang, J.; Gu, S.; Kaspar, R. B.; Zhuang, Z.; Zheng, J.; Guo, H.; Qiu, S.; Yan, Y. 3D Porous Crystalline Polyimide Covalent Organic Frameworks for Drug Delivery. *J. Am. Chem. Soc.* **2015**, *137*, 8352−8355.

(12) Kandambeth, S.; Biswal, B. P.; Chaudhari, H. D.; Rout, K. C.; Kunjattu, S. H.; Mitra, S.; Karak, S.; Das, A.; Mukherjee, R.; Kharul, U. K.; Banerjee, R. Selective Molecular Sieving in Self-Standing Porous Covalent-Organic-Framework Membranes. *Adv. Mater.* **2017**, *29*, DOI: DOI: 10.1002/adma.201603945.

(13) Wu, C.; Liu, Y.; Liu, H.; Duan, C.; Pan, Q.; Zhu, J.; Hu, F.; Ma, X.; Jiu, T.; Li, Z.; Zhao, Y. *J. Am. Chem. Soc.* **2018**, *140*, 10016−10024.

(14) Chen, X.; Addicoat, M.; Irle, S.; Nagai, A.; Jiang, D. Control of Crystallinity and Porosity of Covalent Organic Frameworks by Managing Interlayer Interactions Based on Self-Complementary π-Electronic Force. *J. Am. Chem. Soc.* **2012**, *135*, 546.

(15) Uribe-Romo, F. J.; Doonan, C. J.; Furukawa, H.; Oisaki, K.; Yaghi, O. M. Crystalline Covalent Organic Frameworks with Hydrazone Linkages. *J. Am. Chem. Soc.* **2011**, *133*, 11478−11481.

(16) Kuhn, P.; Antonietti, M.; Thomas, A. Porous, Covalent Triazine-Based Frameworks Prepared by Ionothermal Synthesis. *Angew. Chem., Int. Ed.* **2008**, *47*, 3450−3453.

(17) Tilford, R. W.; Gemmill, W. R.; zur Loye, H.-C.; Lavigne, J. J. Facile Synthesis of a Highly Crystalline, Covalently Linked Porous Boronate Network. *J. Chem. Mater.* **2006**, *18*, 5296−5301.

(18) Wan, S.; Guo, J.; Kim, J.; Ihee, H.; Jiang, D. A Photoconductive Covalent Organic Framework: Self-Condensed Arene Cubes Composed of Eclipsed 2D Polypyrene Sheets for Photocurrent Generation. *Angew. Chem., Int. Ed.* **2009**, *48*, 5439−5442.

(19) Hunt, J. R.; Doonan, C. J.; LeVangie, J. D.; Côté, A. P.; Yaghi, O. M. Reticular Synthesis of Covalent Organic Borosilicate Frameworks. *J. Am. Chem. Soc.* **2008**, *130*, 11872−11873.

(20) Furukawa, H.; Yaghi, O. M. Storage of Hydrogen, Methane, and Carbon Dioxide in Highly Porous Covalent Organic Frameworks for Clean Energy Applications. *J. Am. Chem. Soc.* **2009**, *131*, 8875−8883.

(21) Lanni, L. M.; Tilford, R. W.; Bharathy, M.; Lavigne, J. J. Enhanced Hydrolytic Stability of Self-Assembling Alkylated Two-Dimensional Covalent Organic Frameworks. *J. Am. Chem. Soc.* **2011**, *133*, 13975−13983.

(22) Uribe-Romo, F. J.; Hunt, J. R.; Furukawa, H.; Klöck, C.; O'Keeffe, M.; Yaghi, O. M. A Crystalline Imine-Linked 3-D Porous Covalent Organic Framework. *J. Am. Chem. Soc.* **2009**, *131*, 4570−4571.

(23) Olah, G. A.; Prakash, G. K. S.; Goeppert, A. Anthropogenic Chemical Carbon Cycle for a Sustainable Future. *J. Am. Chem. Soc.* **2011**, *133*, 12881−12898.

(24) Aresta, M.; Dibenedetto, A.; Angelini, A. Catalysis for the Valorization of Exhaust Carbon: from CO_2 to Chemicals, Materials, and Fuels. Technological Use of CO_2. *Chem. Rev.* **2013**, *114*, 1709−1742.

(25) Lee, E.-H.; Ahn, J.-Y.; Dharman, M. M.; Park, D.-W.; Park, S.-W.; Kim, I. Synthesis of cyclic carbonate from vinyl cyclohexene oxide and CO_2 using ionic liquids as catalysts. *Catal. Today* **2008**, *131*, 130−134.

(26) Zhao, Y.; Zhang, J. Effects of ZrO_2 on the Performance of CuO-ZnO-Al_2O_3/HZSM-5 Catalyst for Dimethyl Ether Synthesis from CO_2 Hydrogenation. *J. Nat. Gas Chem.* **2007**, *16*, 389−392.

(27) Buchard, A.; Jutz, F.; Kember, M. R.; White, A. J. P.; Rzepa, H. S.; Williams, C. K. Experimental and Computational Investigation of the Mechanism of Carbon Dioxide/Cyclohexene Oxide Copolymerization Using a Dizinc Catalyst. *Macromolecules* **2012**, *45*, 6781−6795.

(28) Li, Z.; Feng, X.; Zou, Y.; Zhang, Y.; Xia, H.; Liu, X.; Mu, Y. A 2D Azine-Linked Covalent Organic Framework for Gas Storage Applications. *Chem. Commun.* **2014**, *50*, 13825−13828.

(29) Kang, Z.; Peng, Y.; Qian, Y.; Yuan, D.; Addicoat, M. A.; Heine, T.; Hu, Z.; Tee, L.; Guo, Z.; Zhao, D. Mixed Matrix Membranes (MMMs) Comprising Exfoliated 2D Covalent Organic Frameworks (COFs) for Efficient CO_2 Separation. *Chem. Mater.* **2016**, *28*, 1277−1285.

(30) Li, Z.; Zhi, Y.; Feng, X.; Ding, X.; Zou, Y.; Liu, X.; Mu, Y. An Azine-Linked Covalent Organic Framework: Synthesis, Characterization and Efficient Gas Storage. *Chem.—Eur. J.* **2015**, *21*, 12079−12084.

(31) Huang, N.; Chen, X.; Krishna, R.; Jiang, D. Two-Dimensional Covalent Organic Frameworks for Carbon Dioxide Capture through Channel-Wall Functionalization. *Angew. Chem., Int. Ed.* **2015**, *54*, 2986−2990.

(32) Huang, N.; Krishna, R.; Jiang, D. Tailor-Made Pore Surface Engineering in Covalent Organic Frameworks: Systematic Functionalization for Performance Screening. *J. Am. Chem. Soc.* **2015**, *137*, 7079−7082.

(33) Zwaneveld, N. A. A.; Pawlak, R.; Abel, M.; Catalin, D.; Gigmes, D.; Bertin, D.; Porte, L. Organized Formation of 2D Extended

DOI: 10.1021/acsami.8b21867
ACS Appl. Mater. Interfaces 2019, 11, 9343−9354

Covalent Organic Frameworks at Surfaces. *J. Am. Chem. Soc.* **2008**, *130*, 6678−6679.
(34) Liu, X.-H.; Guan, C.-Z.; Ding, S.-Y.; Wang, W.; Yan, H.-J.; Wang, D.; Wan, L.-J. On-Surface Synthesis of Single-Layered Two-Dimensional Covalent Organic Frameworks via Solid-Vapor Interface Reactions. *J. Am. Chem. Soc.* **2013**, *135*, 10470−10474.
(35) Dienstmaier, J. F.; Medina, D. D.; Dogru, M.; Knochel, P.; Bein, T.; Heckl, W. M.; Lackinger, M. Isoreticular Two-Dimensional Covalent Organic Frameworks Synthesized by On-Surface Condensation of Diboronic Acids. *ACS Nano* **2012**, *6*, 7234−7242.
(36) Ascherl, L.; Sick, T.; Margraf, J. T.; Lapidus, S. H.; Calik, M.; Hettstedt, C.; Karaghiosoff, K.; Döblinger, M.; Clark, T.; Chapman, K. W.; Auras, F.; Bein, T. Molecular Docking Sites Designed for The Generation of Highly Crystalline Covalent Organic Frameworks. *Nat. Chem.* **2016**, *8*, 310−316.
(37) Halder, A.; Kandambeth, S.; Biswal, B. P.; Kaur, G.; Roy, N. C.; Addicoat, M.; Salunke, J. K.; Banerjee, S.; Vanka, K.; Heine, T.; Verma, S.; Banerjee, R. Decoding the Morphological Diversity in Two Dimensional Crystalline Porous Polymers by Core Planarity Modulation. *Angew. Chem., Int. Ed.* **2016**, *55*, 7806−7810.
(38) Peng, Y.; Wong, W. K.; Hu, Z.; Cheng, Y.; Yuan, D.; Khan, S. A.; Zhao, D. Room Temperature Batch and Continuous Flow Synthesis of Water-Stable Covalent Organic Frameworks (COFs). *Chem. Mater.* **2016**, *28*, 5095−5101.
(39) Huang, W.; Jiang, Y.; Li, X.; Li, X.; Wang, J.; Wu, Q.; Liu, X. Solvothermal Synthesis of Microporous, Crystalline Covalent Organic Framework Nanofibers and Their Colorimetric Nanohybrid Structures. *ACS Appl. Mater. Interfaces* **2013**, *5*, 8845−8849.
(40) Spitler, E. L.; Dichtel, W. R. Lewis acid-catalysed formation of two-dimensional phthalocyanine covalent organic frameworks. *Nat. Chem.* **2010**, *2*, 672−677.
(41) Chandra, S.; Kandambeth, S.; Biswal, B. P.; Lukose, B.; Kunjir, S. M.; Chaudhary, M.; Babarao, R.; Heine, T.; Banerjee, R. Chemically Stable Multilayered Covalent Organic Nanosheets from Covalent Organic Frameworks via Mechanical Delamination. *J. Am. Chem. Soc.* **2013**, *135*, 17853−17861.
(42) Qian, C.; Xu, S.-Q.; Jiang, G.-F.; Zhan, T.-G.; Zhao, X. Precision Construction of 2D Heteropore Covalent Organic Frameworks by a Multiple-Linking-Site Strategy. *Chem. Eur. J.* **2016**, *22*, 17784−17789.
(43) Zhu, Y.; Shi, J.; Shen, W.; Dong, X.; Feng, J.; Ruan, M.; Li, Y. Stimuli-Responsive Controlled Drug Release from a Hollow Mesoporous Silica Sphere/Polyelectrolyte Multilayer Core-Shell Structure. *Angew. Chem., Int. Ed.* **2005**, *44*, 5083−5087.
(44) Jiang, K.; Zhang, X.; Huang, J.; Wang, S.; Chen, J. Porous Hollow Tubular Carbon Materials Based On Zeolitic Imidazolate Framework-8 Derived From ZnO Nanorods as New Enzyme Immobilizing Matrix for High-Performance Bioanode of Glucose/O_2 Biofuel Cells. *J. Electroanal. Chem.* **2017**, *796*, 88−95.
(45) Lou, X. W.; Archer, L. A.; Yang, Z. Hollow Micro-/Nanostructures: Synthesis and Applications. *Adv. Mater.* **2008**, *20*, 3987−4019.
(46) Hu, L.; Chen, Q. Hollow/porous nanostructures derived from nanoscale metal-organic frameworks towards high performance anodes for lithium-ion batteries. *Nanoscale* **2014**, *6*, 1236−1257.
(47) Zhou, L.; Zhuang, Z.; Zhao, H.; Lin, M.; Zhao, D.; Mai, L. Intricate Hollow Structures: Controlled Synthesis and Applications in Energy Storage and Conversion. *Adv. Mater.* **2017**, *29*, 1602914.
(48) Pachfule, P.; Kandmabeth, S.; Mallick, A.; Banerjee, R. Hollow Tubular Porous Covalent Organic Framework (COF) Nanostructures. *Chem. Commun.* **2015**, *51*, 11717−11720.
(49) Yang, H.; Xiaopo, C.; Xuanxuan, C.; Fusheng, P.; Hong, W.; Guanhua, L.; Yimeng, S.; Xingzhong, C.; Zhongyi, J. Highly Water-Selective Membranes Based on Hollow Covalent Organic Frameworks with Fast Transport Pathways. *J. Membr. Sci.* **2018**, *565*, 331−341.
(50) Kandambeth, S.; Venkatesh, V.; Shinde, D. B.; Kumari, S.; Halder, A.; Verma, S.; Banerjee, R. Self-Templated Chemically Stable Hollow Spherical Covalent Organic Framework. *Nat. Commun.* **2015**, *6*, 6786.
(51) Halder, A.; Kandambeth, S.; Biswal, B. P.; Kaur, G.; Roy, N. C.; Addicoat, M.; Salunke, J. K.; Banerjee, S.; Vanka, K.; Heine, T.; Verma, S.; Banerjee, R. Decoding the Morphological Diversity in Two Dimensional Crystalline Porous Polymers by Core Planarity Modulation. *Angew. Chem., Int. Ed.* **2016**, *55*, 7806−7810.
(52) Gole, B.; Stepanenko, V.; Rager, S.; Grüne, M.; Medina, D. D.; Bein, T.; Würthner, F.; Beuerle, F. Microtubular Self-Assembly of Covalent Organic Frameworks. *Angew. Chem., Int. Ed.* **2017**, *57*, 846−850.
(53) Huo, J.; Wang, L.; Irran, E.; Yu, H.; Gao, J.; Fan, D.; Li, B.; Wang, J.; Ding, W.; Amin, A. M.; Li, C.; Ma, L. Hollow Ferrocenyl Coordination Polymer Microspheres with Micropores in Shells Prepared by Ostwald Ripening. *Angew. Chem., Int. Ed.* **2010**, *49*, 9237−9241.
(54) Li, J.; Zeng, H. C. Hollowing Sn-Doped TiO_2 Nanospheres via Ostwald Ripening. *J. Am. Chem. Soc.* **2007**, *129*, 15839−15847.
(55) Ghosh, S.; Reches, M.; Gazit, E.; Verma, S. Bioinspired Design of Nanocages by Self-Assembling Triskelion Peptide Elements. *Angew. Chem., Int. Ed.* **2007**, *46*, 2002−2004.
(56) Lou, X. W.; Archer, L. A.; Yang, Z. Hollow Micro-/Nanostructures: Synthesis and Applications. *Adv. Mater.* **2008**, *20*, 3987−4019.
(57) EL-Mahdy, A. F. M.; Kuo, C.-H.; Alshehri, A.; Young, C.; Yamauchi, Y.; Kim, J.; Kuo, S.-W. Strategic Design of Triphenylamine- and Triphenyltriazine-Based Two-Dimensional Covalent Organic Frameworks for CO_2 Uptake and Energy Storage. *J. Mater. Chem. A.* **2018**, *6*, 19532−19541.
(58) Zhai, L.; Ning, H.; Hong, X.; Qiuhong, C.; Donglin, J. A backbone design principle for covalent organic frameworks: the impact of weakly interacting units on CO_2 adsorption. *Chem. Commun.* **2017**, *53*, 4242−4245.
(59) Gao, Q.; Xing, L.; Guo-Hong, N.; Hai-Sen, X.; Cuibo, L.; Bingbing, T.; Wei, T.; Kian, P. L. Covalent Organic Framework with Frustrated Bonding Network for Enhanced Carbon Dioxide Storage. *Chem. Mater.* **2018**, *30*, 1762−1768.
(60) Huang, N.; Chen, X.; Krishna, R.; Jiang, D. Two-dimensional covalent organic frameworks for carbon dioxide capture through channel-wall functionalization. *Angew. Chem., Int. Ed.* **2015**, *54*, 2986−2990.
(61) Hsiao, S.-H.; Lin, S.-W. Electrochemical Synthesis of Electrochromic Polycarbazole Films from N-Phenyl-3,6-bis(N-carbazolyl)carbazoles. *Polym. Chem.* **2016**, *7*, 198−211.
(62) Khattak, A. M.; Ghazi, Z. A.; Liang, B.; Khan, N. A.; Iqbal, A.; Li, L.; Tang, Z. A Redox-Active 2D Covalent Organic Framework with Pyridine Moieties Capable of Faradaic Energy Storage. *J. Mater. Chem. A.* **2016**, *4*, 16312−16317.
(63) Su, C.; Yang, F.; Ji, L.; Xu, L.; Zhang, C. Polytriphenylamine Derivative with High Free Radical Density as The Novel Organic Cathode for Lithium Ion Batteries. *J. Mater. Chem. A.* **2014**, *2*, 20083−20088.
(64) Su, C.; He, H.; Xu, L.; Zhao, K.; Zheng, C.; Zhang, C. A Mesoporous Conjugated Polymer Based on A High Free Radical Density Polytriphenylamine Derivative: Its Preparation and Electrochemical Performance as A Cathode Material for Li-Ion Batteries. *J. Mater. Chem. A.* **2017**, *5*, 2701−2709.
(65) Li, J.; Zan, G.; Wu, Q. An Ultra-High-Performance Anode Material for Supercapacitors: Self-Assembled Long Co_3O_4 Hollow Tube Network with Multiple Heteroatom (C-, N- and S-) Doping. *J. Mater. Chem. A.* **2016**, *4*, 9097−9105.
(66) Hryniewicz, B. M.; Winnischofer, H.; Vidotti, M. Interfacial Characterization and Supercapacitive Behavior of PEDOT Nanotubes Modified Electrodes. *J. Electroanal. Chem.* **2018**, *823*, 573−579.
(67) Yu, Z.; Tetard, L.; Zhai, L.; Thomas, J. Supercapacitor Electrode materials: Nanostructures from 0 to 3 Dimensions. *Energy Environ. Sci.* **2015**, *8*, 702−730.
(68) Li, X.-C.; Zhang, Y.; Wang, C.-Y.; Wan, Y.; Lai, W.-Y.; Pang, H.; Huang, W. Redox-active triazatruxene-based conjugated micro-

DOI: 10.1021/acsami.8b21867
ACS Appl. Mater. Interfaces 2019, 11, 9343−9354

porous polymers for high-performance supercapacitors. *Chem. Sci.* **2017**, *8*, 2959−2965.
(69) DeBlase, C. R.; Silberstein, K. E.; Truong, T.-T.; Abruña, H. D.; Dichtel, W. R. β-Ketoenamine-Linked Covalent Organic Frameworks Capable of Pseudocapacitive Energy Storage. *J. Am. Chem. Soc.* **2013**, *135*, 16821−16824.
(70) DeBlase, C. R.; Hernández-Burgos, K.; Silberstein, K. E.; Rodríguez-Calero, G. G.; Bisbey, R. P.; Abruña, H. D.; Dichtel, W. R. Rapid and Efficient Redox Processes within 2D Covalent Organic Framework Thin Films. *ACS Nano* **2015**, *9*, 3178−3183.
(71) Halder, A.; Ghosh, M.; Khayum M, A.; Bera, S.; Addicoat, M.; Sasmal, H. S.; Karak, S.; Kurungot, S.; Banerjee, R. Interlayer Hydrogen-Bonded Covalent Organic Frameworks as High-Performance Supercapacitors. *J. Am. Chem. Soc.* **2018**, *140*, 10941−10945.
(72) Chandra, S.; Roy Chowdhury, D.; Addicoat, M.; Heine, T.; Paul, A.; Banerjee, R. Molecular Level Control of the Capacitance of Two-Dimensional Covalent Organic Frameworks: Role of Hydrogen Bonding in Energy Storage Materials. *Chem. Mater.* **2017**, *29*, 2074−2080.
(73) Khayum M, A.; Vijayakumar, V.; Karak, S.; Kandambeth, S.; Bhadra, M.; Suresh, K.; Acharambath, N.; Kurungot, S.; Banerjee, R. Convergent Covalent Organic Framework Thin Sheets as Flexible Supercapacitor Electrodes. *ACS Appl. Mater. Interfaces* **2018**, *10*, 28139−28146.

DOI: 10.1021/acsami.8b21867
ACS Appl. Mater. Interfaces 2019, 11, 9343−9354